Journal of the Optical Society of America B
OPTICAL PHYSICS

Time-domain Fabry–Perot resonators formed inside a dispersive medium

J. Zhang,[1,*] W. R. Donaldson,[2] and Govind P. Agrawal[1,2]

[1]The Institute of Optics, University of Rochester, Rochester, New York 14627, USA
[2]Laboratory for Laser Energetics, University of Rochester, Rochester, New York 14623, USA
*Corresponding author: jzh156@ur.rochester.edu

Received 19 April 2021; revised 15 June 2021; accepted 3 July 2021; posted 4 July 2021 (Doc. ID 428411); published 26 July 2021

We show that the temporal analog of a Fabry–Perot resonator (FPR) can be realized by using two moving temporal boundaries, formed by intense pump pulses inside a dispersive medium (such as an optical fiber). We analyze such FPRs using a transfer-matrix method, similar to that used for spatial structures containing multiple thin films. We consider a temporal slab formed using a single square-shape pump pulse and find that the resonance of such an FPR has transmission peaks whose quality (Q) factors decrease rapidly with an increasing velocity difference between the pump and probe pulses. We propose an improved design by using two pump pulses. We apply our transfer-matrix method to this design and show considerable improvement in the Q factors of various peaks. We also show that such FPRs can be realized in practice by using two short pump pulses that propagate as solitons inside a fiber. We verified the results of the transfer-matrix method by directly solving the pulse propagation equation with the split-step Fourier method.

https://doi.org/10.1364/JOSAB.428411

1. INTRODUCTION

Temporal variations in the refractive index of a dielectric medium are useful for a variety of applications, including optical signal processing. Reflection of optical fields at a temporal boundary with different refractive indices on its two sides has attracted attention in several contexts [1–14]. A stationary boundary is often employed, assuming that the refractive index changes suddenly at all spatial points at the same time. However, such a temporal boundary is not easy to realize in practice, and the dispersion of the medium is usually not considered. A moving temporal boundary was employed in [5] to study the temporal reflection of optical pulses inside a dispersive medium. It was found that the spectra of reflected and refracted pulses shifted from the spectrum of the incident pulse in such a way that the reflected part never crossed the boundary, even though all parts of the original pulse moved in the same direction. A moving temporal boundary can be realized in experiments using the nonlinear phenomenon of cross-phase modulation [15] induced by a pump pulse, or by applying a microwave pulse to a traveling-wave phase modulator.

The properties of a new kind of material, known as the space-time metamaterial, have been studied in recent years [7–9]. A time-domain laser cavity was also studied in [10]. The cavity was formed in time domain by temporal reflection. A pulse train can be generated from the cavity. Another interesting development is related to a device called a time-domain Fabry–Perot resonator (FPR). It is formed by two temporal boundaries separated in time and its properties were recently studied [11]. This idea has also been extended to the temporal analog of a device made with multiple thin films of different dielectric materials [12]. However, all films were assumed to be dispersion-free, without any frequency dependence of the refractive indices. In this work, we consider a temporal FPR built by using two moving temporal boundaries inside an optical waveguide (such as an optical fiber) and includes the full effects of group-velocity dispersion (GVD). We developed a transfer matrix method and used it to explain the behaviors of temporal FPR.

Recently, we developed an analytic approach to study temporal reflection at a moving boundary [16]. In Section 2, we use this approach and present a transfer-matrix method for time-domain FPRs that is similar to the method used to find the reflectivity of a structure containing multiple thin films. In Section 3, we discuss the similarity and differences between the spatial and temporal FPRs. In Section 4, we study a temporal FPR formed using two short pump pulses separated in time by a fixed duration. As an example, we found that a FPR formed by two solitons works quite well. This configuration was numerically considered earlier with less attention to the FPR resonances and the reflectivity spectrum [13]. The main results of our paper are summarized in Section 5.

2. TRANSFER-MATRIX METHOD

We consider the propagation of an optical pulse (called the probe) inside a dispersive medium, such as a single-mode fiber. We ignore all spatial effects, assuming that the pulsed beam

maintains its spatial dimensions, but include the frequency dependence of the refractive index $n(\omega)$. To simplify the problem, we expand the propagation constant, $\beta(\omega) = (\omega/c)n(\omega)$, of the optical mode in a Taylor series as

$$\beta(\omega) = \beta_0 + \beta_1(\omega - \omega_0) + \frac{1}{2}\beta_2(\omega - \omega_0)^2, \tag{1}$$

where ω_0 is a reference frequency near the central frequency of the pulse. Note that it does not have to be the central frequency. We neglected the third- and higher-order dispersion terms in the Taylor expansion, assuming that the input spectrum is relatively narrow compared to its central frequency. The parameter β_1 is related inversely to the group velocity of the pulse, and β_2 is known as the GVD parameter [15]. The refractive index can be made time dependent by injecting intense pump pulses together with the probe pulse. Each pump pulse changes the refractive index by a small amount through the nonlinear Kerr effect only over its duration. We include such changes through $\beta_0'(t) = \beta_0 + b(t)$, where $b(t) = (\omega_0/c)\Delta n(t)$ and $\Delta n(t)$ is the change in the refractive index induced by a pump pulse.

To study the evolution of the probe pulse, we work in a frame where the pump pulses traveling with the speed V_p appear stationary. Introducing $t = t' - z/V_p$, where t' is the time in the laboratory frame, the evolution of the probe pulse is governed by [5]

$$\frac{\partial A}{\partial z} + \Delta\beta_1\frac{\partial A}{\partial t} + i\frac{\beta_2}{2}\frac{\partial^2 A}{\partial t^2} = ib(t)A, \tag{2}$$

where $A(z, t)$ is the slowly varying amplitude of the probe pulse and $\Delta\beta_1 = \beta_1 - 1/V_p$. The electric field is related to A through $E(z, t') = A(z, t')\exp[i(\beta_0 z - \omega_0 t')]$. The preceding equation is similar to the nonlinear Schrödinger equation and can be solved with the split-step Fourier method [15].

To solve Eq. (2) analytically, we work in the spectral domain and separately consider each frequency component of the Fourier spectrum. Second, we divide the time window over which $b(t) \neq 0$ into small segments such that $b(t)$ can be treated as a constant in each segment. We can use this procedure for any form of $b(t)$ provided we make segments relatively short when $b(t)$ changes rapidly. In the nth segment, we can set $b(t) = b_n$ in Eq. (2). The resulting equation has an analytic solution in the form of a plane wave:

$$A(z, t) = A_0\exp[i(\Delta\beta_n z - \Delta\omega_n t)], \tag{3}$$

where $\Delta\omega_n$ is the frequency shift in the nth segment (from the reference frequency ω_0) and the change in propagation constant in this segment is given by

$$\Delta\beta_n = b_n + \Delta\beta_1\Delta\omega_n + \frac{1}{2}\beta_2\Delta\omega_n^2. \tag{4}$$

It is known from earlier work that the propagation constant is preserved across a temporal boundary [5]. This requirement implies that $\Delta\beta_n$ should be the same in all segments. Because $b(t)$ is induced by a pump pulse, it is nonzero only over the duration of this pulse. Consider a specific spectral component at the frequency $\omega_0 + \Delta\omega_+$. Just before it arrives at the first segment, where $b(t) = 0$ because the pump pulse is absent, Eq. (4) leads to

$$\Delta\beta_0 = \Delta\beta_1\Delta\omega_+ + \frac{1}{2}\beta_2\Delta\omega_+^2. \tag{5}$$

Because the propagation constant should be the same in all segments, we can use $\Delta\beta_n = \Delta\beta_0$. Using this result in Eq. (4), the frequency shift in each segment is found to be

$$\Delta\omega_{n,\pm} = \frac{1}{\beta_2}\left[-\Delta\beta_1 \pm \sqrt{(\Delta\beta_1 + \beta_2\Delta\omega_+)^2 - 2b_n\beta_2}\right]. \tag{6}$$

The physical meaning of these two solutions can be understood by noting that a plane wave incident on the nth segment undergoes temporal reflection and refraction, resulting in two plane waves of different frequencies. These waves travel at different speeds because of the GVD such that one of them travels slower than the incoming wave. In the moving frame used here, this wave appears to be moving backward.

Accounting for both plane waves, the general solution of Eq. (2) in the nth segment should be written as

$$A(t) = A_+(t) + A_-(t) = A_+e^{-i\Delta\omega_{n,+}t} + A_-e^{-i\Delta\omega_{n,-}t}, \tag{7}$$

where we suppress the dependence on z to simplify the notation. We can use this equation to relate the amplitudes at the two ends of the nth segment of duration $\tau_n = t_{n+1} - t_n$. The resulting matrix relation is found to be

$$\begin{pmatrix} A_+(t_n) \\ A_-(t_n) \end{pmatrix} = \begin{pmatrix} e^{i\Delta\omega_{n,+}\tau_n} & 0 \\ 0 & e^{i\Delta\omega_{n,-}\tau_n} \end{pmatrix}\begin{pmatrix} A_+(t_{n+1}) \\ A_-(t_{n+1}) \end{pmatrix}. \tag{8}$$

The next step is to find the transfer matrix between two neighboring segments. For this purpose, we make use of the boundary conditions across a temporal boundary. These require that both A and $\partial A/\partial t$ should be continuous across the boundary. If we denote the amplitudes on the two sides of the boundary with $A(t)$ and $A'(t)$ and write them as superpositions of the two plane waves of different frequencies as indicated in Eq. (7), we obtain

$$A_+ + A_- = A'_+ + A'_-, \tag{9}$$

$$\Delta\omega_+A_+ + \Delta\omega_-A_- = \Delta\omega'_+A'_+ + \Delta\omega'_-A'_-. \tag{10}$$

Solving the linear equations, we can write the result in the form

$$\begin{pmatrix} A_+ \\ A_- \end{pmatrix} = \begin{pmatrix} \frac{\Delta\omega'_+ - \Delta\omega_-}{\Delta\omega_+ - \Delta\omega_-} & \frac{\Delta\omega'_- - \Delta\omega_-}{\Delta\omega_+ - \Delta\omega_-} \\ \frac{\Delta\omega_+ - \Delta\omega'_+}{\Delta\omega_+ - \Delta\omega_-} & \frac{\Delta\omega_+ - \Delta\omega'_-}{\Delta\omega_+ - \Delta\omega_-} \end{pmatrix}\begin{pmatrix} A'_+ \\ A'_- \end{pmatrix}. \tag{11}$$

This equation can be simplified considerably by noting from Eq. (6) that $\Delta\omega_+ + \Delta\omega_- = -2\Delta\beta_1/\beta_2$. The same is true for $\Delta\omega'_+$ and $\Delta\omega'_-$. Thus, we have $\Delta\omega_+ + \Delta\omega_- = \Delta\omega'_+ + \Delta\omega'_-$. Using these relations, Eq. (11) can be rewritten as

$$\begin{pmatrix} A_+ \\ A_- \end{pmatrix} = \frac{1}{\tau}\begin{pmatrix} 1 & \rho \\ \rho & 1 \end{pmatrix}\begin{pmatrix} A'_+ \\ A'_- \end{pmatrix}, \tag{12}$$

where we have defined the temporal amplitude reflection and transmission coefficients as

$$\rho = \frac{\Delta\omega_+ - \Delta\omega'_+}{\Delta\omega'_+ - \Delta\omega_-}, \quad \tau = \frac{\Delta\omega_+ - \Delta\omega_-}{\Delta\omega'_+ - \Delta\omega_-}. \tag{13}$$

We can now follow the same procedure that is used in the spatial case of a structure containing multiple thin films. In fact, our transfer matrix in Eq. (12) is written in the same form used for the spatial case. The only difference is that frequencies are involved in our case whereas angles are involved in the spatial case. This is an example of space-time duality that has been exploited for temporal imaging using a time lens [17].

3. TEMPORAL SLAB

In the spatial case, a dielectric slab with two partially reflecting ends forms a FPR such that its transmission becomes 100% at specific frequencies that correspond to its resonances. A temporal slab provides the simplest example of a time-domain FPR. It is made by using two temporal boundaries such that the refractive index is different inside the region separating these boundaries from that outside of it. Assuming that the temporal slab occupies the region $0 < t < T$, the function $b(t)$ in Eq. (2) has the form

$$b(t) = \begin{cases} b_0 & 0 < t < T, \\ 0 & \text{otherwise.} \end{cases} \tag{14}$$

We denote the frequencies outside the slab as $\Delta\omega_{\pm}$ and the frequencies inside the slab as $\Delta\omega'_{\pm}$. Physically, a plane wave with frequency $\Delta\omega_+$ propagates in the $t < 0$ region and its frequency changes to $\Delta\omega'_+$ at the boundary at $t = 0$. This wave gets reflected at the boundary at $t = T$ and its frequency changes to $\Delta\omega'_-$. Some part of this reflected wave enters the region $t < 0$ and its frequency changes to $\Delta\omega_-$. This process is exactly like what happens in a spatial slab. So, for resonance to occur, the reflected waves from the two boundaries must interfere destructively. This can only happen if $\Delta\omega'_{\pm}$ is real.

We use the transfer-matrix method developed in Section 2 to find the transmission coefficient of the temporal slab and determine the condition for resonance to occur with 100% transmission through the slab. We denote the reflection and transmission coefficients at the boundary $t = 0$ as ρ and τ, and at the boundary $t = T$ as ρ' and τ'. It is easy to show that $\rho' = -\rho$. Similar to the spatial case, the transfer matrix of the temporal slab is found by multiplying the following matrices:

$$\begin{aligned} M &= \frac{1}{\tau}\begin{pmatrix} 1 & \rho \\ \rho & 1 \end{pmatrix}\begin{pmatrix} e^{i\Delta\omega'_+ T} & 0 \\ 0 & e^{i\Delta\omega'_- T} \end{pmatrix}\frac{1}{\tau'}\begin{pmatrix} 1 & -\rho \\ -\rho & 1 \end{pmatrix}, \\ &= \frac{1}{\tau\tau'}\begin{pmatrix} e^{i\Delta\omega'_+ T} - \rho^2 e^{i\Delta\omega'_- T} & -\rho(e^{i\Delta\omega'_+ T} - e^{i\Delta\omega'_- T}) \\ \rho(e^{i\Delta\omega'_+ T} - e^{i\Delta\omega'_- T}) & e^{i\Delta\omega'_- T} - \rho^2 e^{i\Delta\omega'_+ T} \end{pmatrix}. \end{aligned} \tag{15}$$

The wave amplitudes on the two sides of the temporal slab are related to the matrix elements M_{ij} as

$$\begin{pmatrix} A_+(0) \\ A_-(0) \end{pmatrix} = \begin{pmatrix} M_{11} & M_{12} \\ M_{21} & M_{22} \end{pmatrix}\begin{pmatrix} A_+(T) \\ 0 \end{pmatrix}. \tag{16}$$

It follows that the reflection and transmission coefficients of a temporal slab are given by

$$\rho_{\text{slab}} = \frac{A_-(0)}{A_+(0)} = \frac{M_{21}}{M_{11}}, \tag{17}$$

$$\tau_{\text{slab}} = \frac{A_+(T)}{A_+(0)} = \frac{1}{M_{11}}. \tag{18}$$

Using M_{11} from Eq. (15), the transmissivity of the slab is found to be

$$T_{\text{slab}} = |\tau_{\text{slab}}|^2 = \left(1 + \frac{4|\rho|^2}{(1-|\rho|^2)^2}\sin^2[(\Delta\omega'_+ - \Delta\omega'_-)T/2]\right)^{-1}. \tag{19}$$

This expression has the same form as the one found for a space-domain slab acting as an FPR. Similar to the spatial case, multiple peaks with 100% transmission occur when the resonance condition, $(\Delta\omega'_+ - \Delta\omega'_-)T = 2m\pi$, is satisfied, where m is an integer. Also, similar to a spatial FPR, the larger is the value of $|\rho|^2$ or T, the sharper the transmission peak becomes, and the higher is the Q factor of that peak. However, there is one critical feature that makes a temporal slab quite different from a spatial slab: Whereas the reflectivity $|\rho|^2$ at the two interfaces is nearly constant over a wide spectral range in the spatial case, it changes rapidly in the temporal cases because $|\rho|^2$ depends on the incident frequency $\Delta\omega_+$.

To quantify the impact of this critical difference, Fig. 1 shows both $|\rho|^2$ and T_{slab} as a function of normalized frequency shift defined as $\Delta f = (\beta_2/\Delta\beta_1)\Delta\omega_+$ using a specific set of parameter values: $\Delta\beta_1 = 0.1$ ps/m, $\beta_2 = 0.005$ ps^2/m, $b_0 = 1.2$ m^{-1}, and $T = 1$ ps. As seen there, multiple transmission peaks do occur but their Q factors and shapes vary so much that only a few resonances exist that are not even equally spaced. The first peak is the narrowest because $|\rho|^2$ is the largest in its vicinity (about 55%). The second peak is broader because $|\rho|^2$ is about 32% in its vicinity. For the same reason, the transmission does not drop to zero between two neighboring peaks. These features are quite different from the spatial case in which all transmission peaks have nearly the same contrast and the same Q factor.

Another noteworthy feature of a temporal slab is the presence of a frequency range over which $|\rho|^2$ becomes 100% because of total internal reflection (TIR). In this case, the frequency shifts $\Delta\omega'_{\pm}$ inside the slab become imaginary, resulting in the formation of evanescent waves decaying exponentially with time.

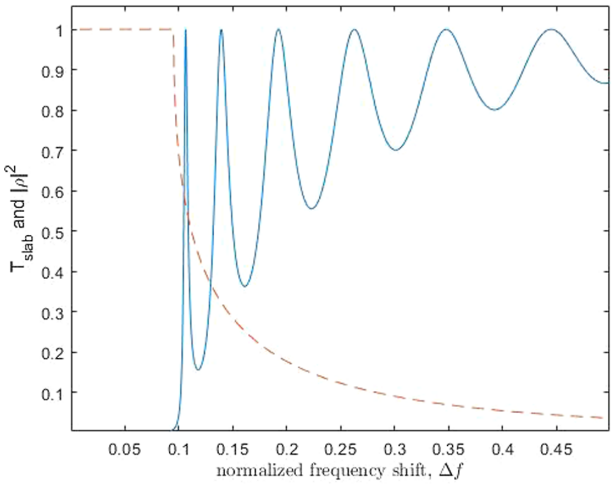

Fig. 1. Transmissivity of the temporal slab (solid line) and reflectivity of its front boundary (dashed line).

However, for a sufficiently narrow slab (duration T relatively small), the temporal analog of frustrated TIR can still occur.

The results seen in Fig. 1 can be used to understand how an incoming pulse splits into the reflected and transmitted parts as it crosses a temporal slab. We first find the spectral contents of the incoming pulse by using the Fourier transform

$$\tilde{A}_{in}(\omega) = \int_{-\infty}^{\infty} A_{in}(t) e^{i\omega t} \mathrm{d}t. \tag{20}$$

The amplitudes of the reflected and transmitted pulses are calculated by considering refection and transmission of individual frequency components and then taking the inverse Fourier transform:

$$A_r(t) = \frac{1}{2\pi} \int_{-\infty}^{\infty} \rho_s(\omega) \tilde{A}_{in}(\omega) e^{-i\omega t} \mathrm{d}\omega, \tag{21}$$

$$A_t(t) = \frac{1}{2\pi} \int_{-\infty}^{\infty} \tau_s(\omega) \tilde{A}_{in}(\omega) e^{-i\omega t} \mathrm{d}\omega, \tag{22}$$

where ω plays the role of the frequency shift $\Delta\omega_+$. Alternatively, we can solve Eq. (2) numerically with $b(t)$ given in Eq. (14).

We used the split-step Fourier method [15] to solve Eq. (2) numerically. We chose the same parameter values used for Fig. 1 and assumed a Gaussian input pulse using $A_{in}(t) = \exp(-t^2/2T_0^2)$ with $T_0 = 20$ ps. Figs. 2(a) and 2(b) show two cases at different wavelengths for the index change shown in Fig. 2(c). The dashed lines in Figs. 2(a) and 2(b) mark the position of the temporal slab. Note that the temporal slab over which index changes does not vary with z in the moving frame. Fig. 2(d) shows that the pulse's spectrum is centered at the second transmission peak in Fig. 2(a) and at the first transmission valley in Fig. 2 (b). In both cases, temporal evolution of the pulse is shown over a distance of 2 km. This distance is long but feasible in practice when optical fibers are used for the dispersive medium. A higher-index region at $t = 60$ps forms a temporal slab whose duration is much narrower (1 ps) compared to the pulse width. The value $b_0 = 1.2\ \mathrm{m}^{-1}$ inside this slab region corresponds to an index change of only 3×10^{-7} and can be realized in practice using a short, intense pump pulse with a duration of 1 ps.

Figure 2(a) shows that the pulse reaches the front boundary at a distance of 500 m and reaches the other end of the slab after a short distance. The important feature is that more than 90% of the pulse energy is transmitted through the slab when the pulse's spectrum is centered at a resonance of the FPR formed by the slab. The reason that some energy (about 7%) is reflected is related to the finite distance it takes for the pulse to cross the slab. Indeed, we see two reflected pulses that correspond to reflections at the two interfaces of the slab. The situation in Fig. 2(b) is quite different when compared to Fig. 2(a). In this case, the reflected pulse contains most of the input energy. This is expected from Fig. 2(c), where we see that the reflectivity is about 84% at the first valley. We note that the reflected pulses appear to be moving toward the negative time ($t = 0$ corresponds to the peak of input pulse). This is not a violation of causality because t is a relative time in a frame in which that temporal slab is stationary. Physically, when the probe pulse crosses the pump pulse (the temporal slab), a part of the probe pulse changes its frequency so that it speeds up and appears to move away from the pump pulse.

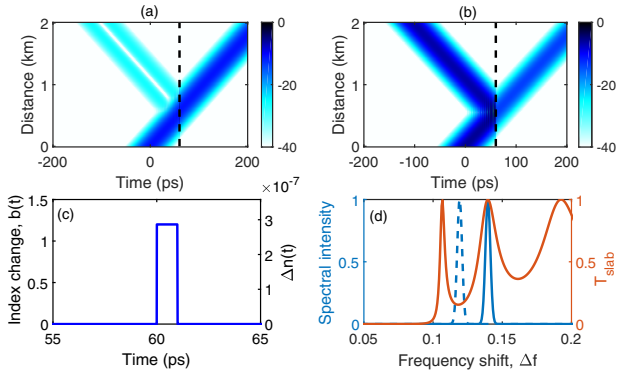

Fig. 2. Temporal evolution of a 20 ps Gaussian pulse when its spectrum is centered at (a) the second transmission peak and (b) the first minimum. The dashed lines in (a) and (b) represent the position of the temporal slab. (c) Temporal window over which the refractive index change occurs. (d) Location of pulse spectra within the transmission curve (red) of the temporal slab. Blue solid line is the incident spectrum of (a) and dashed line is the incident spectrum of (b); spectral intensity is plotted for convenience.

4. IMPROVED TIME-DOMAIN FPRS

We saw in Section 3 that a temporal window, with a higher (or lower) refractive index compared to its surroundings, behaves like a FPR in the time domain. However, its resonances are not uniform because the reflection coefficient of each temporal boundary exhibits a strong frequency dependence. As a result, its transmission peaks have low Q factors and their contrast (difference between the transmission's peak and valley) diminishes after one or two peaks. We show in this section that FPRs with high Q factors can be designed by using two temporal slabs separated in time. In practice, this configuration can be realized by using two identical pump pulses that serve as two high-reflectivity mirrors of a temporal FPR. The exact shape of two pump pulses is not important, but it should not change much as these pulses propagate inside the dispersive medium. This feature suggests immediately the use of optical solitons for making such FPRs [13].

We use the transfer-matrix method developed in Sections 2 and 3 to understand the properties of the proposed FPR, shown schematically in Fig. 3 using two identical pump pulses. As pulse shapes will be different in practice, we develop our theory for an arbitrary shape of pump pulses. We denote the elements of the transfer matrix of a single pump pulse as M_{11}, M_{12}, M_{21}, and M_{22}. These elements are functions of the frequency shift $\Delta\omega_+$ and can be calculated by dividing the pump pulses into many segments and multiplying the matrices.

The transfer matrix of the FPR shown in Fig. 3 is obtained by multiplying the following three matrices:

$$M_{FP} = \begin{pmatrix} M_{11} & M_{12} \\ M_{21} & M_{22} \end{pmatrix} \begin{pmatrix} e^{i\Delta\omega_+ T} & 0 \\ 0 & e^{i\Delta\omega_- T} \end{pmatrix} \begin{pmatrix} M_{11} & M_{12} \\ M_{21} & M_{22} \end{pmatrix}. \tag{23}$$

It follows from Eq. (18) that the transmissivity of the FPR is given by

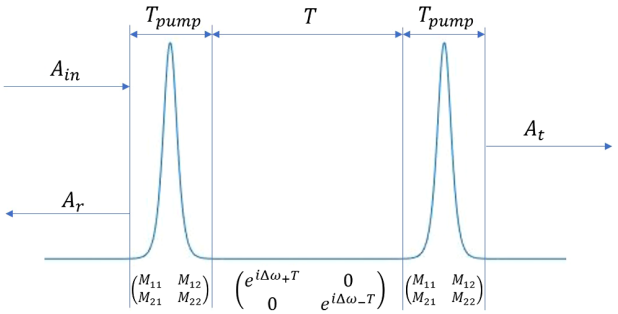

Fig. 3. Design of the proposed time-domain FPR. Two identical pump pulses of duration T_{pump}, separated by an interval T, act as temporal mirrors. The bottom part shows the transfer matrices of three sections.

$$T_{FP} = |M_{11}^2 e^{i\Delta\omega T} + M_{12}M_{21}|^{-2}, \tag{24}$$

where $\Delta\omega = \Delta\omega_+ - \Delta\omega_-$. Using the relation (see Supplement 1)

$$\begin{pmatrix} M_{11} & M_{12} \\ M_{21} & M_{22} \end{pmatrix} = \begin{pmatrix} M_{22}^* & M_{21}^* \\ M_{12}^* & M_{11}^* \end{pmatrix} \exp\left[-i\frac{2\Delta\beta_1}{\beta_2} T_{\text{pump}}\right], \tag{25}$$

we can simplify T_{FP} as

$$T_{FP} = \left(1 + \frac{4|\Gamma|^2}{(1-|\Gamma|^2)^2}\sin^2\frac{\phi}{2}\right)^{-1}, \tag{26}$$

where $\Gamma = M_{21}/M_{11}$ is the amplitude reflection coefficient of a single pump pulse,

$$\phi = \Delta\omega T + 2\Delta\beta_1 T_{\text{pump}}/\beta_2 + 2\phi_0 - \pi, \tag{27}$$

and ϕ_0 is the phase of complex number M_{11}. Equation (26) has the same functional form as Eq. (19), except that the bandwidth of each transmission peak width depends on the temporal reflectivity $|\Gamma|^2$ of each pump pulse, instead of a single boundary. This feature improves the performance of the proposed FPR because $|\Gamma|^2$ usually changes less rapidly with frequency than the reflectivity of a single temporal boundary and allows the formation of several more narrowband transmission peaks.

To illustrate the performance of the proposed FPR, we consider a practical configuration: The pump pulse's wavelength is in the anomalous region of the optical fiber while the probe pulse is in the normal dispersion region. The two pump pulses propagate as two optical solitons and their center is delayed by T_c [15]. A high-index region forms over the width of each pulse because of a Kerr-induced increase in the refractive index of the fiber's mode. In this case, $b(t)$ in Eq. (2) has the form

$$b(t) = b_0\left[\text{sech}^2\left(\frac{t}{T_0}\right) + \text{sech}^2\left(\frac{t-T_c}{T_0}\right)\right]. \tag{28}$$

As an example, we choose $\Delta\beta_1$, β_2 the same as in Fig. 1 and set b_0 to 1.2 m^{-1}, which corresponds to a maximum index increase of only $\Delta n = 3\times10^{-7}$. We use $T_0 = 50$ fs and $T_c = 1.4$ ps. We calculated the transfer matrix of each pump pulse by dividing it into 500 segments from $-4T_0$ to $4T_0$. We used this matrix to calculate both $|\Gamma|^2$ and the transmissivity T_{FP} of the FPR, and the results are shown in Fig. 4.

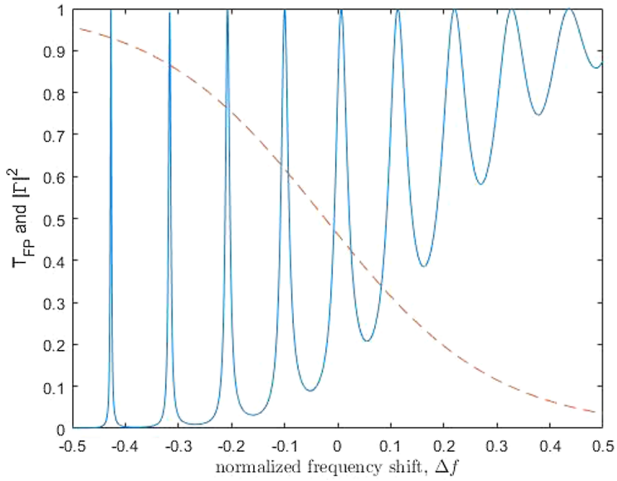

Fig. 4. Frequency dependence of T_{FP} (solid line) and $|\Gamma|^2$ (dashed line) for a temporal FPR formed using two pump pulses propagating as solitons inside an optical fiber.

A comparison of Figs. 1 and 4 shows the improvement realized by using two solitons as temporal boundaries of an FPR. Similar to the single-slab case, there are multiple transmission peaks in Fig. 4, but they are much sharper (narrower) compared to the slab case and thus have high Q factors. This difference can be solely attributed to the frequency dependence of $|\Gamma|^2$ compared to that of a single, sharp temporal boundary. The reflectivity of a relatively short soliton (FWHM about 90 fs) varies smoothly with frequency and remains >50% over a large frequency range, resulting in the several sharp transmission peaks seen in Fig. 4.

Just as was done in Fig. 2, we simulated the transmission of a probe pulse through the FPR at the peak and valley of one transmission peak in Fig. 4 by numerically solving Eq. (2). We used a Gaussian-shape probe pulse with $T_0 = 20$ ps, and the results are shown in Figs. 5(a) and 5(b). Figure 5(c) shows the refractive index changes in the time domain and Fig. 5(d) shows the locations of the probe spectra in Figs. 5(a) and 5(b).

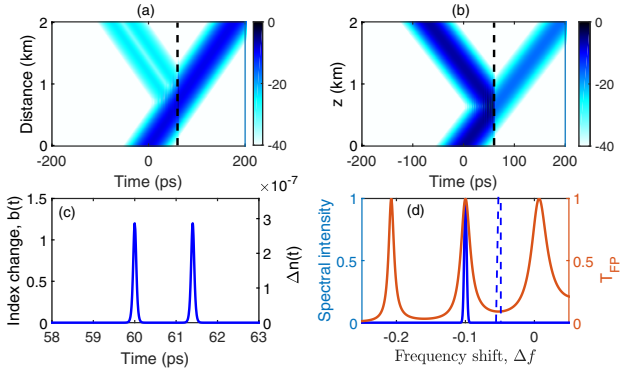

Fig. 5. Temporal evolution of a 20 ps Gaussian pulse when its spectrum is centered at (a) a transmission peak and (b) a transmission valley. The dashed lines in (a) and (b) represent the position of the temporal FPR. (c) Refractive index changes in the time domain. (d) Location of pulse spectra within the transmission curve (red) of the FPR. Blue solid line is the incident spectrum in (a) and the dashed line is the incident spectrum in (b); spectral intensity is plotted.

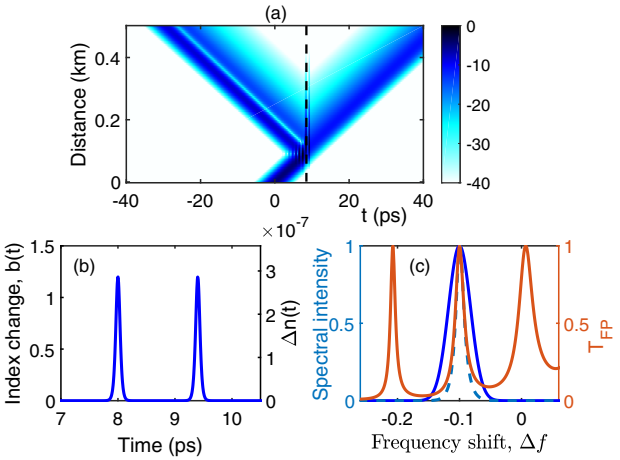

Fig. 6. (a) Temporal evolution of a 2 ps Gaussian pulse when two pump pulses change the refractive index in time domain, as shown in (b). The dashed lines in (a) represent the location of the temporal FPR. The probe pulse's spectrum is centered at a transmission peak of the FPR. (c) Spectra of the incident (blue solid line) and transmitted pulses (blue dashed line) superposed on the transmission curve of the FPR (red).

As predicted by our transfer-matrix method, the probe pulse is almost completely transmitted when its spectrum is centered at the transmission peak. In contrast, it is mostly reflected when its spectrum is centered at the transmission valley. In both cases, there is some energy leakage due to the finite width of the resonator. The reason for almost perfect transmission and reflection is related to a relatively large width of the probe pulse, chosen to ensure a narrow spectrum that fits within the bandwidth of the transmission peak.

When the probe pulse becomes shorter than 10 ps, its spectrum becomes wider than the transmission peak, and the FPR behaves like an optical filter. To verify this, we simulated the case of a probe pulse with $T_0 = 2$ ps, and the results are shown in Fig. 6. Pump-induced temporal changes in the refractive index are shown in Fig. 6(b). We see in Fig. 6(a) that only a fraction of the pulse's energy is transmitted even though the pulse's spectrum is centered at the peak with 100% transmission. This is because the probe spectrum is wider than the transmission peak, as seen in Fig. 5(c), resulting in a significant amount of reflection. Both the reflected and transmitted pulses have long tails, caused by multiple reflections occurring inside the FPR. Figure 6(c) shows the spectrum of the transmitted pulse together with the transmission curve of the FPR. The transmitted spectrum is narrower than that of the incident pulse and fits within the transmission peak, as expected on the physical ground. These results indicate clearly that a temporal FPR can be used as an optical filter.

5. CONCLUSION

In this paper, we show that the temporal analog of a FPR can be realized by using two moving temporal boundaries inside a dispersive medium such as an optical fiber. In practice, such boundaries are created using a pump-probe configuration in which one or more short pump pulses are launched together with a probe pulse. Each pump pulse increases the refractive index of the single mode of the fiber through the nonlinear Kerr effect, but this increase lasts only over the duration of the pump pulse.

To calculate the transmissive properties of such time-domain FPRs, we develop a transfer-matrix method similar to that used to analyze the reflectivity of a spatial structure containing multiple thin films. We show that this method can be used to calculate the transfer matrix of pump pulses of any shape. As a simple example, we first consider a temporal slab formed by using a single pump pulse with sharp leading and trailing edges (a rectangular shape pulse) and acting as a simple FPR. We found that such an FPR has several transmission peaks corresponding to resonances similar to that occurring in spatial FPRs, but the bandwidth (or Q factor) and contrast of these peaks decrease rapidly with increasing frequency. The reason behind this behavior is related to the reflection coefficient of each boundary that forms a slab. In contrast to the spatial FPRS for which the mirror's reflectivity remains constant over a wide bandwidth, temporal reflection is very sensitive to the frequency of incident light.

We propose what we believe, to the best of our knowledge, is an improved design for time-domain FPRs using two temporally separated pump pulses so that each pump pulse acts as a reflective element of the FPR. We apply our transfer-matrix method to this design for pulses of arbitrary shapes and obtain an expression for the transmissivity of such FPRs that appears identical to the corresponding result for space-domain FPRs. We also show that temporal FPRs formed in the anomalous-GVD region of optical fibers by using two short solitons to form multiple sharp transmission peaks with relatively high Q factors. We verified the results of the transfer-matrix method by directly solving the pulse propagation equation with the split-step Fourier method. We showed that that a probe pulse can be totally transmitted through such an FPR when its spectrum overlaps with that of a transmission peak of the FPR. If the spectrum width is larger than the transmission peak width, the temporal FPR acts like an optical filter, just as its spatial counterpart.

Even though we used the Kerr effect as an example of changing the refractive index inside an optical fiber to present our numerical results, a planar waveguide can also be used for experimental realization of a temporal FPR. In particular, the use of a silicon waveguide may allow the refractive index to be changed electrically using a p-n junction. The refractive index can also be changed electrically inside a lithium-niobate waveguide using the electro-optic effect.

Funding. National Science Foundation (ECCS-1933328).

Disclosures. The authors declare no conflicts of interest.

Data Availability. Data underlying the results presented in this paper are not publicly available at this time but may be obtained from the authors upon reasonable request.

Supplemental document. See Supplement 1 for supporting content.

REFERENCES

1. J. T. Mendonça and P. K. Shukla, "Time refraction and time reflection: two basic concepts," Phys. Scr. **65**, 160–163 (2002).
2. M. Notomi and S. Mitsugi, "Wavelength conversion via dynamic refractive index tuning of a cavity," Phys. Rev. A **73**, 051803 (2006).

3. F. Biancalana, A. Amann, A. V. Uskov, and E. P. O'Reilly, "Dynamics of light propagation in spatiotemporal dielectric structures," Phys. Rev. E **75**, 046607 (2007).
4. Y. Xiao, D. N. Maywar, and G. P. Agrawal, "Reflection and transmission of electromagnetic waves at a temporal boundary," Opt. Lett. **39**, 574–577 (2014).
5. B. W. Plansinis, W. R. Donaldson, and G. P. Agrawal, "What is the temporal analog of reflection and refraction of optical beams," Phys. Rev. Lett. **115**, 183901 (2015).
6. D. K. Kalluri, *Electromagnetics of Time Varying Complex Media: Frequency and Polarization Transformer*, 2nd ed. (CRC, 2016).
7. C. Caloz and Z.-L. Deck-Léger, "Spacetime metamaterials. Part I: general concepts," IEEE Trans. Antennas Propag. **68**, 1569–1582 (2020).
8. C. Caloz and Z.-L. Deck-Léger, "Spacetime metamaterials–Part II: Theory and applications," IEEE Trans. Antennas Propag. **68**, 1583–1598 (2020).
9. V. Pacheco-Peña and N. Engheta, "Temporal aiming," Light Sci. Appl. **9**, 129 (2020).
10. A. C. Sparapani, A. D. Sánchez, N. Linale, J. Bonetti, D. F. Grosz, and G. R. Fernández, "All-optical pulse-train generation through the temporal analogue of a laser," in *Frontiers in Optics Technical Digest* (Optical Society of America, 2020), paper JTh4A.41.
11. D. Ramaccia, A. Toscano, and F. Bilotti, "Light propagation through metamaterial temporal slabs: reflection, refraction, and special cases," Opt. Lett. **45**, 5836–5839 (2020).
12. D. Ramaccia, A. Alù, A. Toscano, and F. Bilotti, "Temporal multilayer structures for designing higher-order transfer functions using time-varying metamaterials," Appl. Phys. Lett. **118**, 101901 (2021).
13. T. Voytova, I. Oreshnikov, A. V. Yulin, and R. Driben, "Emulation of Fabry–Perot and Bragg resonators with temporal optical solitons," Opt. Lett. **41**, 2442–2445 (2016).
14. H. Chen, C. Qin, B. Wang, and P. Lu, "Discrete refraction and reflection in temporal lattice heterostructures," Opt. Lett. **44**, 363–366 (2019).
15. G. P. Agrawal, *Nonlinear Fiber Optics*, 6th ed. (Academic, 2019).
16. J. Zhang, W. Donaldson, and G. P. Agrawal, "Temporal reflection and refraction of optical pulses inside a dispersive medium: An analytic approach," J. Opt. Soc. Am. B **38**, 997–1003 (2021).
17. B. H. Kolner and M. Nazarathy, "Temporal imaging with a time lens," Opt. Lett. **14**, 630–632 (1989).